

# Radio Frequency Interference Mitigation for the Planned SMAP Radar and Radiometer

Michael Spencer, Samuel Chan, Eric Belz  
Jet Propulsion Laboratory, California Institute of Technology

Jeffrey Piepmeier, Priscilla Mohammed, Edward Kim  
NASA's Goddard Space Flight Center

Joel T. Johnson  
The Ohio State University

## ABSTRACT

NASA's planned SMAP<sup>1</sup> mission will utilize a radar operating in a band centered on 1.26 GHz and a co-observing radiometer operating at 1.41 GHz to measure surface soil moisture. Both the radar and radiometer sub-systems are susceptible to radio frequency interference (RFI). Any significant impact of such interference requires mitigation in order to avoid degradation in the SMAP science products. Studies of RFI detection and mitigation methods for both the radar and radiometer are continuing in order to assess the risk to mission products and to refine the performance achieved.

**Index Terms**— SMAP, Radar, Radiometer, RFI

## 1. INTRODUCTION

Anthropogenic radio emissions are a known contamination source for both passive and active remote sensing. Both airborne and spaceborne systems have shown the L-Band spectral region to be susceptible. As shown in Figure 1, the SMAP radar [1] operates in a shared band where other terrestrial and spaceborne emitters are allowed to legally operate. The SMAP radiometer nominally operates in a protected band, but unauthorized in-band sources as well as spectral spillover from adjacent bands are observed to cause interference.

<sup>1</sup> The SMAP mission has not been formally approved by NASA. The decision to proceed with the mission will not occur until the completion of the National Environmental Policy Act (NEPA) process. Material in this document related to SMAP is for information purposes only.

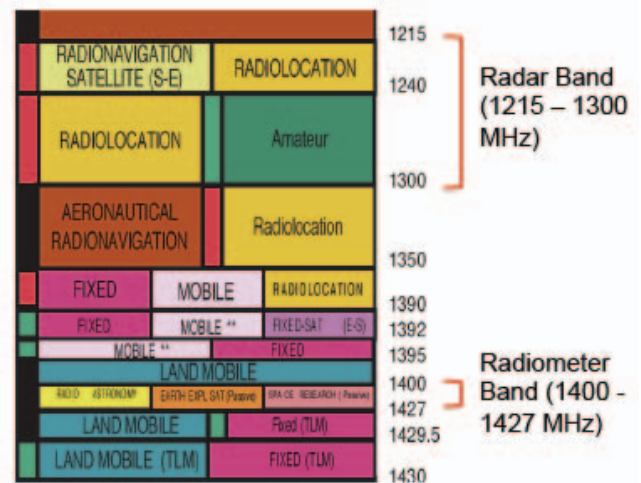


Figure 1: L-band frequency allocations with SMAP radar and radiometer frequencies indicated.

## 2. SMAP RADAR RFI

Contamination due to the presence of RFI is a known error source for remote sensing radars. Most potential interfering emissions at L-Band are relatively narrow band. Because the SMAP radar itself is a narrow band system (1 MHz linear chirp), a key RFI avoidance strategy for SMAP is to make the center transmit frequency adjustable. If persistent RFI is encountered in a given band over a given region, the center frequency is simply commanded to a different location in the spectrum.

Despite best efforts to operate the SMAP radar in a "clear" band, it is inevitable that some RFI contamination will be observed. Therefore, RFI detection and removal will be performed as part of

ground data processing [2]. Developing and assessing the necessary processing algorithms requires a characterization of the expected RFI environment to be encountered.

RFI can be divided into two sources: ground-based sources and space-based sources. Ground-based sources are expected to create the most interference. There are essentially two methods available to characterize the properties of ground-based interference. The first is to use data from current space-based and airborne systems operating at L-Band (such as ALOS/PALSAR and UAVSAR). The second is to attempt to model RFI using the characteristics of known emitters. An examination of currently operating L-Band systems indicates that approximately 87% of RFI is from “pulsed” sources, and 13% is from “other” sources such as continuous wave (CW) emitters. RFI modeling studies have thus far been restricted to known U.S. and Canadian long-range tracking radars. A significant effort has been exerted to collect a comprehensive database of these emitters, and to model the resulting interference power. When such a simulation is performed, it is estimated that approximately 10% of all SMAP synthetic aperture radar intervals can be expected to have interference that exceeds the required 0.4 dB error when the surface has a relatively low backscatter cross-section (-25 dB).

The primary detection/correction algorithm that has been demonstrated for pulsed interferers is the so-called “Slow-Time Thresholding” or STT algorithm. Here, the fact that the pulse repetition frequency (PRF) of RFI signals is usually slow relative to the SMAP PRF is leveraged. The STT technique essentially looks at the slow-time series associated with a given range bin, sets an appropriate threshold, and flags any azimuth samples that exceed this threshold as RFI events. To the extent that the total number of RFI events is small ( $< 15$ ), the scene can be processed with these specific azimuth samples removed. A survey of PALSAR data shows that the vast majority of SMAP synthetic aperture intervals will have five or fewer RFI events that would be flagged by STT. These studies also show that when the flagged samples are excised, the residual measurement error associated with the “cleansed” scene is less than 0.1 dB (see Figure 2).

The only space-based sources that will generate significant RFI contamination are Global Navigation Satellite Systems (GNSS). The characteristic feature

of GNSS is that they emit low, continuous, wide-band interference, which appears noise-like in the relatively narrow SMAP bandwidth. GNSS interference can enter the SMAP receiver through the backlobes and by specular or diffuse scattering off of the surface.

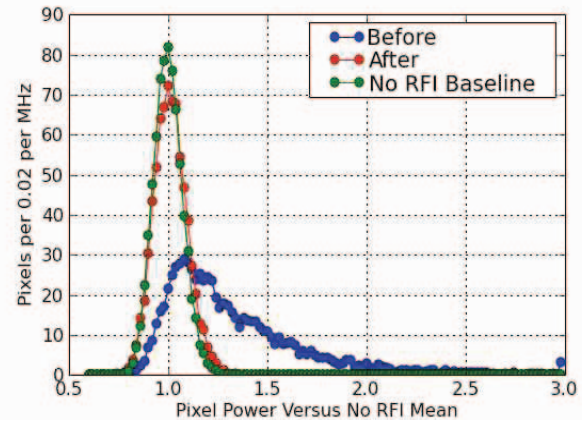


**Figure 2: Simulated STT algorithm performance showing minimal change in backscattering coefficient following STT processing vs. control .**

Modeling has been performed for the GPS constellation and the SMAP backlobe antenna pattern. Because the GNSS signals are constant in time (or at least constant over a synthetic aperture time), the interference can basically be treated as a rise in the background noise, analogous to a rise in the thermal noise power. In general, the GNSS interference power is actually several dB below the normal thermal noise power, so it is not a large effect. Nevertheless, it is a non-negligible effect if not compensated for. The normal noise-only measurement and subsequent noise subtraction step during SMAP radar processing provides a “built in” technique to remove the contamination. The technique works well where the GNSS spectrum is relatively flat (i.e., in the M- and P-Code portions of the GPS spectrum), but does not work well where the spectrum is narrow (i.e., the C-Code portion of the spectrum). It is found that direct GNSS interference can be removed to within 0.1 dB and 0.2 dB for the lowest co-pol and lowest cross-pol signals respectively if the GPS spectral region around 1227.5 MHz is avoided.

The reflection of GNSS signals from the Earth’s surface is another mechanism for RFI contamination of the SMAP radar measurement. This mechanism has the potential to create the greatest levels of interference because the SMAP antenna boresight, and

hence the highest antenna gain, is pointed at the Earth. The probability of receiving uncorrectably high levels of interference has been estimated at about 2% of all the data if it is assumed that the Earth acts as a perfect specularly reflecting surface. Of course, the Earth mostly does not behave in such a specular fashion, so in reality the resultant data loss will be much lower ( $\ll 1\%$ ). The more general case of diffuse scattering is currently being studied.

### 3. SMAP RADIOMETER RFI

Although international regulations prohibit sources from operating directly within the 1400-1427 MHz protected portion of the spectrum, spurious emission from sources outside the band as well as potential illegal emissions present at these frequencies exists. Any RFI power present in the 24 MHz bandwidth of the SMAP radiometer will positively bias the observed brightness temperature, resulting in an erroneous dry bias in soil moisture estimates if uncorrected. While large RFI impacts ( $> \sim 40\text{-}50\text{K}$ ) can be detected and discarded, thereby causing data loss, smaller RFI contributions are more difficult to detect and more likely to impact science products. An error budget produced by the SMAP Science Definition Team characterizes RFI corruption of even  $\sim 0.5\text{K}$  as significant. The SMAP radiometer will therefore include a digital receiver to enable advanced RFI detection and mitigation strategies.

As with the SMAP radar, an extensive effort has been conducted to characterize the expected RFI environment to be encountered by the SMAP radiometer. Two primary sources of RFI information have been utilized: a set of airborne observations in the United States [3] and observations of ESA's SMOS L-band radiometer [4]. Results from [3] obtained from advanced RFI characterization systems included in the campaign show a variety of sources to be present, including both pulsed and narrowband, with some limited evidence of "broadband" continuous sources. SMOS data do not provide detailed RFI source information, but do provide a global characterization of observed RFI power levels. In particular, SMOS data show increased RFI levels in global regions outside the Americas. Current RFI characterization efforts are attempting to scale RFI properties observed in the airborne campaigns to be compatible with the global distribution of brightness temperatures observed by SMOS.

The characterization data available shows sources typically to be either pulsed or narrow-band (i.e. CW-like) in nature. As with the radar's STT approach, pulsed sources can be detected in the time-domain if the radiometer detector is sampled at a sufficiently high temporal resolution. The SMAP radiometer has a fundamental sampling frequency at the radar PRF of 3.2 kHz, which allows ground-based sub-millisecond RFI detection and mitigation using simple "pulse" strategies [5]. To detect and mitigate CW sources, the radiometer's 24 MHz bandwidth is digitally filtered into  $16 \times 1.5$  MHz sub-bands (see Fig. 3). Detected powers in these sub-bands will also be telemetered to the ground at  $\sim 1$  msec temporal resolution. The resulting  $\sim 1.5$  MHz  $\times$  1 msec spectrogram dataset can be utilized in a variety of RFI detection methods, including channelized pulse detection, cross-frequency algorithms [6], or "peak-picking" methods [5].

In addition to time/frequency discrimination, the radiometer digital subsystem will also compute the first through fourth moments of observed fields both in the 24 MHz "fullband" (i.e. 3.2 kHz) and 1.5 MHz "sub-band" (16 channel  $\times$  1 msec) datasets. The availability of these moments will enable computation of the fullband and sub-band kurtosis for RFI detection [7]-[8], which has also been shown effective against several source types. Finally, the radiometer will also measure fully polarimetric information (all four Stokes parameters), enabling additional polarimetric RFI detection strategies. Current research is investigating appropriate strategies for combining the outputs of the multiple detectors that are possible on this multi-stream (i.e. corresponding fullband and sub-band datasets representing the same observation) product. A maximum-likelihood strategy is currently under investigation for this algorithm.

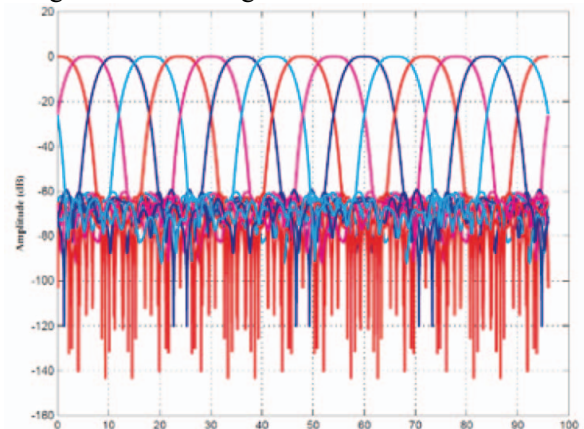
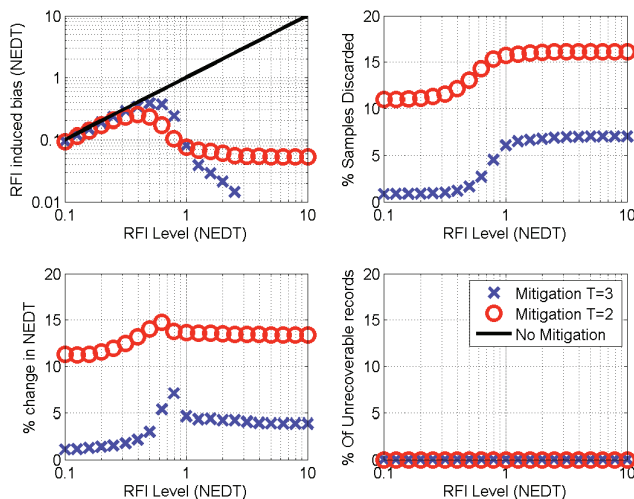


Figure 3: Radiometer sub-bands.

Figure 4 provides an example of the potential performance for a subset of SMAP radiometer RFI detection algorithms. A Monte Carlo simulation of the SMAP fullband data stream was performed in the presence of an interfering pulsed source producing 2 micro-sec pulses at a rate such that 2 pulses are encountered in the 8 millisecond integration period considered. Power levels of the interferer are varied from 0.1 to 10 times a nominal  $\sim 1\text{K}$  radiometer NEDT. Biases in estimated brightness temperatures are computed in 1000 Monte Carlo trials following application of the RFI detection and mitigation strategy. In this case, the detection strategy is an “or” of the fullband pulse and kurtosis detection methods. Two differing threshold levels (T) for the algorithms are compared, with smaller T values producing more sensitive detection but higher false alarm rates.

Computed results for the RFI induced bias (upper left), % of 3.2 kHz samples discarded (upper right), % change in NEDT (lower left), and % of unrecoverable records (lower right) all show the capability of these algorithms for producing RFI induced errors  $< \sim 0.5\text{ K}$  for the full range of source amplitudes considered. Continued studies are in progress to incorporate a wide variety of source types and information on the global distribution of source amplitudes.



**Figure 4: Monte Carlo simulation of expected SMAP radiometer detection and mitigation performance versus RFI power for a 2 micro-sec pulsed source. Algorithm is an “or” of “fullband” pulse and kurtosis detectors. Upper left: RFI induced bias; Upper Right: % of 3.2 kHz samples discarded; Lower left: Change in radiometer sensitivity following mitigation; Lower right: % of unrecoverable 8 millisecond integration periods.**

## REFERENCES

- [1] D. Entekhabi et al, “The Soil Moisture Active Passive (SMAP) mission,” *Proc. IEEE*, vol. 98, pp. 704–716, 2010.
- [2] S. Chan and M. Spencer, “RFI Study for the SMAP Radar,” *Proceedings of the IEEE Radar Conference, Pasadena, CA, May*, 2009.
- [3] J. Park et al, “Airborne L-band RFI observations from the SMAPVEX08 campaign and associated flights,” accepted by *IEEE Trans. Geosc. Rem. Sens.*, 2011.
- [4] A. Camps et al, “RFI analysis in SMOS imagery,” *Proc. IGARSS 2010*, 2010.
- [5] J. T. Johnson and L. C. Potter, “A study of detection algorithms for pulsed sinusoidal interference in microwave radiometry,” *IEEE Trans. Geosc. Rem. Sens.*, vol. 47, pp. 628–636, 2009.
- [6] B. Guner and J. T. Johnson, “Performance study of a cross-frequency detection algorithm for pulsed sinusoidal RFI in microwave radiometry,” *IEEE Trans. Geosc. Rem. Sens.*, vol. 48, pp. 2899–2908, 2010.
- [7] C. S. Ruf, S. M. Gross, S. Misra, “RFI detection and mitigation for microwave radiometry with an agile digital detector,” *IEEE Trans. Geosc. Rem. Sens.*, vol. 44, pp. 694–706, 2006.
- [8] S. Misra et al, “Microwave radiometer RFI Detection Algorithms: a comparative study,” *IEEE Trans. Geosc. Rem. Sens.*, vol. 47, pp. 3742–3754, 2009.

## Acknowledgments

Research in this paper was performed at NASA’s Goddard Space Flight Center. Research described in this paper was also carried out at the Jet Propulsion Laboratory, California Institute of Technology, under a contract with the National Aeronautics and Space Administration.